Multifunctional Material for Organic Electronics

Bull. Korean Chem. Soc. **2013**, Vol. 34, No. 5   1355

A Multifunctional Material Based on Triphenylamine and a Naphthyl Unit for Organic Light-Emitting Diodes, Organic Solar Cells, and Organic Thin-Film Transistors

Jongchul Kwon, Myoung Ki Kim, Jung-Pyo Hong, Woochul Lee, Seonghoon Lee, and Jong-In Hong[*]

Department of Chemistry, College of Natural Sciences, Seoul National University, Seoul 151-747, Korea
[*]E-mail: jihong@snu.ac.kr

We have developed a new multifunctional material, 4,4',4''-tris(4-naphthalen-2-yl-phenyl)amine (**2-TNPA**), which can be used as a blue-emitting and hole-transporting material in organic light-emitting diodes (OLEDs), as well as a donor material in organic solar cells (OSCs) and an active material in organic thin-film transistors (OTFTs). The OLED device doped with 3% **2-TNPA** shows a maximum current efficiency of 3.0 cdA^{-1} and an external quantum efficiency of 3.0%. **2-TNPA** is a more efficient hole-transporting material than 4,4'-bis[*N*-(naphthyl-*N*-phenylamino)]biphenyl (NPD). Furthermore, **2-TNPA** shows a power-conversion efficiency of 0.39% in OSC and a field-effect mobility of 3.2×10^{-4} cm^{2}V^{-1}s^{-1} in OTFTs.

Key Words : Multifunctional materials, Organic light-emitting diode, Organic solar cells, Organic thin-film transistor

Introduction

Since the introduction of organic electronics such as organic solar cells (OSCs),[1a] organic light-emitting diodes (OLEDs),[1b] and organic thin-film transistors (OTFTs),[1c] the development of organic electronics has attracted considerable attention because of their low cost, easy device fabrication, flexible panels, and potential applications such as OLED displays, solar cells, electronic sensors, and radio-frequency identification tags (RFIDs). Small-molecule-based organic electronics[2] have been widely investigated for opto-electronic applications in OSCs,[3] as light-emitting[4] and hole-transporting[5] materials in OLEDs, and in OTFTs[6] because of their light absorption, light-emitting, and hole-transporting, and charge carrier-transport properties, repectively.

Some of the important factors in the manufacturing process of organic electronic devices are the low cost and the simple device fabrication. For example, one important application of multifunctional materials is in the manufacture of RFIDs using a printing process.[7a] The RFID-manufacturing technology comprises power devices, transistors, and displays, all integrated into a plastic foil or paper. Considering the fact that the fabrication of each individual device would require a series of more than 10 patterning, material deposition, and post-processing steps, the manufacture of RFID devices would require more than 50 manufacturing steps, making the cost of RFID technology prohibitive. To overcome this problem, Berggren and coworkers introduced multifunctional materials for organic electronics such as OSCs, OLEDs, and OTFTs.[7a] Generally, such materials must have light-emitting, light-absorption, and charge carrier-transporting properties for use in OLEDs, OSCs, and OTFTs, respectively. Since the operation mechanisms of OLEDs, OSCs, and OTFTs are different, it is generally difficult to use the same organic materials as active layers in all devices. For
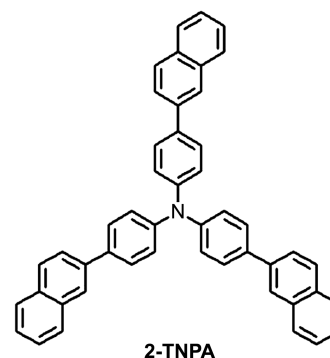

Figure 1. Molecular structure of **2-TNPA**.

this reason, only a few bifunctional[8] or trifunctional[9] organic materials have been developed so far. Recently, multifunctional materials have been reported for light-emitting materials in OLEDs, donor materials in OSCs, and active channels in OTFTs.[10]

In this paper, we report a new multifunctional material, 4,4',4''-tris(4-naphthalen-2-yl-phenyl)amine (**2-TNPA**, Figure 1), which can be used as a blue-emitting and hole-transporting material in OLEDs, a donor material in OSCs, and an active material in OTFTs. The OLED device doped with 3% **2-TNPA** shows a maximum current efficiency of 3.0 cdA^{-1} and an external quantum efficiency of 3.0%. **2-TNPA** shows more efficient hole-transporting properties when compared to 4,4'-bis[*N*-(naphthyl-*N*-phenylamino)]biphenyl (NPD). Furthermore, **2-TNPA** shows a power-conversion efficiency of 0.39% in OSC and a field-effect mobility (μ) of 3.2×10^{-4} cm^{2}V^{-1}s^{-1} in OTFT.

Experimental

Materials and Instruments. Organic compounds such as

2,9-dimethyl-4,7-diphenyl-1,10-phenanthroline (BCP), NPD, tris(8-hydroxyquinolinato)aluminum (Alq$_3$), fullerene (C$_{60}$), copper phthalocyanine (CuPc), poly(3,4-ethylenedioxy thiophene)poly(styrenesulfonate) (PEDOT:PSS), 9,10-di(2-naphthyl)anthracene (ADN), tris(4-bromophenyl)amine, and 2-naphthaleneboronic acid were purchased from Tokyo Chemical Industry (TCI), Aldrich, Baytron, Lumtree, and Gracel Display. Analytical thin layer chromatography was performed using Kieselgel 60F-254 plates from Merck. Column chromatography was carried out on Merck silica gel 60 (70230 mesh). All solvents and reagents were commercially available and used without further purification unless otherwise noted. ^{1}H and ^{13}C NMR spectra were recorded using an Avance 300 or 500 MHz Bruker spectrometer in CDCl$_3$. ^{1}H NMR chemical shifts in CDCl$_3$ were referenced to CHCl$_3$ (7.27 ppm), and ^{13}C NMR chemical shifts in CDCl$_3$ were reported relative to CHCl$_3$ (77 ppm). Absorption (UV) spectra were recorded on a Beckman DU 650 spectrophotometer. Photoluminescence (PL) spectra were recorded on a Jasco FP-7500 spectrophotometer. Cyclic voltammetry (CV) spectra were obtained using a CH Instruments 660 electrochemical analyzer. Atomic Force Microscope (AFM) experiments were performed using an Asylum MFP-3D instrument in AC mode, and XRD analyses were carried out using a Rigaku (λ = 1.5418 Å; 298 K) X-ray instrument. Decomposition temperatures (T_d) were obtained using a thermal gravimetric analyzer (TGA) from a Q5000IR TGA instrument. Glass transition temperatures (T_g) were obtained using a differential scanning calorimeter (DSC) from DSCQ1000 instrument.

Synthesis. 4,4',4"-Tris(4-naphthalen-2-yl-phenyl)amine (**2-TNPA**): A mixture of tris(4-bromophenyl)amine (2.00 g, 4.14 mmol), 2-naphthaleneboronic acid (2.50 g, 14.5 mmol), potassium carbonate (2 M, 20 mL), and palladium tetrakisphenyl phosphonate (238 mg, 0.206 mmol) in THF/H$_2$O was heated at 80 °C for 72 h. After cooling to room temperature, all the volatiles were evaporated under vacuum and the reaction mixture was extracted with dichloromethane. The organic phase was washed with water and dried over MgSO$_4$. The solvent was evaporated to give the crude product, which was purified by silica gel column chromatography using a mixture of ethyl acetate and hexane as the eluent (1:10), and then recrystallized from dichloromethane and hexane to give a solid product (yield: 700 mg, 27%). ^{1}H NMR (300 MHz, CDCl$_3$) δ 8.08 (s, 3H), 7.93 (d, 15 Hz, 6H), 7.88 (d, 3 Hz, 3H), 7.79 (d, 9 Hz, 3H), 7.70 (d, 18 Hz, 6H), 7.52 (d, 18 Hz, 6H), 7.36 (d, 9 Hz, 6H). ^{13}C NMR (125 MHz, CDCl$_3$) δ 147.1, 138.1, 135.7, 133.9, 132.6, 128.6, 128.4, 128.3, 127.8, 126.5, 125.9, 125.5, 125.3, 124.7. Mass: calcd. for C$_{48}$H$_{33}$N [M]$^+$ 623.2613, HR-Mass: 623.2616.

Cyclic Voltammetry. The electrochemical experiment was referenced with respect to silver/silver chloride (Ag/AgCl) as the reference electrode at room temperature, and then calibrated using a ferrocene/ferrocenium (Fc/Fc$^+$). The CH$_2$Cl$_2$ solution for CV contained a glassy carbon working electrode, a platinum wire counter electrode, and a 0.1 M tetra-*n*-butylammonium hexafluorophosphate (TBAPF$_6$) as a sup-

porting electrolyte.

Blue-Emitting OLED Device Fabrication. A 10-nm-thick layer of CuPc was used as a hole-injection layer, and a 60-nm-thick layer of NPD was used as a hole-transporting layer. A 50-nm-thick emitting layer was prepared using ADN as a host and 3-5 wt % **2-TNPA** as a fluorescent blue dopant. Next, a 20-nm-thick Alq$_3$ layer, which served as an electron-transporting layer, was evaporated, followed by the evaporation of LiF, which served as an electron-injection layer. Finally, a 100-nm-thick Al layer was deposited on the LiF layer.
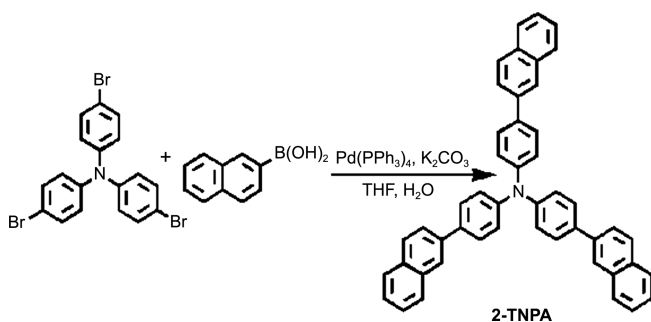
Green-Emitting OLED Device Fabrication. We fabricated two types of green-fluorescent OLEDs, which comprised either a 70-nm-thick NPD layer or a 70-nm-thick **2-TNPA** layer as a hole-transporting layer. Next, a 60-nm-thick Alq$_3$ layer was evaporated as an electron-transporting layer and a green-emitting layer. Then, LiF, used as an electron-injection layer, was evaporated, followed by a 100-nm-thick Al layer deposited on the LiF layer.

OSC Device Fabrication. A 30-nm-thick PEDOT:PSS layer was used as a hole-injection layer. Various **2-TNPA** layers with thicknesses varying from 10 nm to 20 nm were prepared by evaporation. Then, a 40-nm-thick C$_{60}$ layer, which served as an acceptor, was evaporated, followed by the evaporation of a 5-nm-thick BCP layer, which served as an exciton-blocking layer. Finally, a 100-nm-thick Al layer was evaporated on the BCP layer.

OTFT Device Fabrication. The transistors based on **2-TNPA** were fabricated with the top-contact geometry. We used a heavily doped Si wafer as the gate electrode and an un-pretreated or an octadecyltrichlorosilane (OTS)-pretreated SiO$_2$ layer (thickness, *ca.* 300 nm) as the gate dielectric. **2-TNPA** (*ca.* 50 nm) was grown by vacuum-sublimation, using a home-made apparatus, at a rate of 0.4-0.8 Ås^{-1} under a working pressure of 2.0-2.5×10^{-6} torr. Gold source/drain electrodes were evaporated on top of the films through a shadow mask with a channel length (L) of 50 μm and a channel width (W) of 1000 μm. Electrical characterization of the transistors was performed at room temperature in air using a Keithley 4200-SCS semiconductor analyzer. The value of μ was calculated in the saturation region ($V_{DS} = -100$ V) from the plot of the square-root of drain current *vs.* V_{GS} using the following equation: $I_{DS} = (WC_i\mu(V_{GS}-V_T)^2)/2L$, where I_{DS} is the source-drain saturation current; C_i (1.1×10^{-8} F) is the capacitance of the SiO$_2$ insulator; W/L is the ratio of the width to the channel length; and V_{GS} and V_T are the gate-source and threshold voltages (V_{th}), respectively.

Results and Discussion

2-TNPA was synthesized by a one-step palladium-catalyzed Suzuki cross-coupling reaction between tris(4-bromophenyl)amine and 2-naphthaleneboronic acid (Scheme 1). The photophysical properties of **2-TNPA** are shown in Figure 2. The absorption spectrum of **2-TNPA** in CH$_2$Cl$_2$ shows intense bands at 283 and 361 nm. Absorption at 361 nm corresponds to the π-π* transition of the triphenylamine

Scheme 1. Synthesis of **2-TNPA**.

Figure 4. Blue-emitting OLED devices with a configuration of ITO/CuPc (10 nm)/NPD (60 nm)/EML (50 nm)/Alq$_3$ (20 nm)/LiF (1 nm)/Al (100 nm). (a) EL spectra. (b) Current density (mAcm^{-2}) *vs.* current efficiency (cdA^{-1}) characteristics.

unit, while the short wavelength band at 283 nm originates from the electronic transitions of the naphthyl unit. The PL spectrum of **2-TNPA** in CH$_2$Cl$_2$ shows blue emission centered at 440 nm, with the full width at half maximum (FWHM) of 64 nm. The PL quantum yield of **2-TNPA** in CH$_3$CH$_2$OH was estimated to be 0.24 using anthracene as a standard. The thermal stability of **2-TNPA** was investigated using TGA and DSC, and its thermal decomposition temperature (T_d) was determined as 455 °C (Figure S7). In DSC experiments, **2-TNPA** shows amorphous glassy properties with T_g of 95 °C (Figure S8). The electrochemical properties of **2-TNPA** were measured by CV in CH$_2$Cl$_2$. Figure 3 shows the cyclic voltammogram of 0.1 mM **2-TNPA** in CH$_2$Cl$_2$. **2-TNPA** undergoes a reversible oxidation process associated with
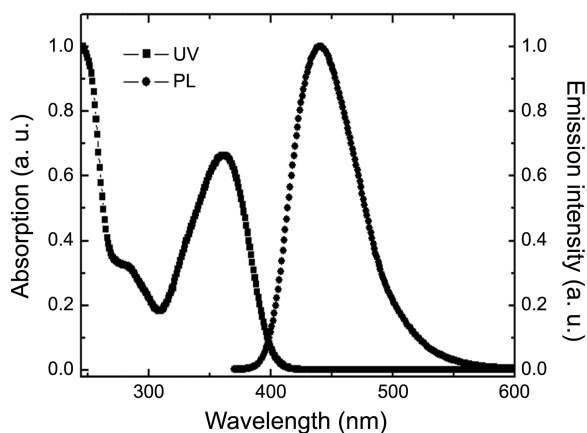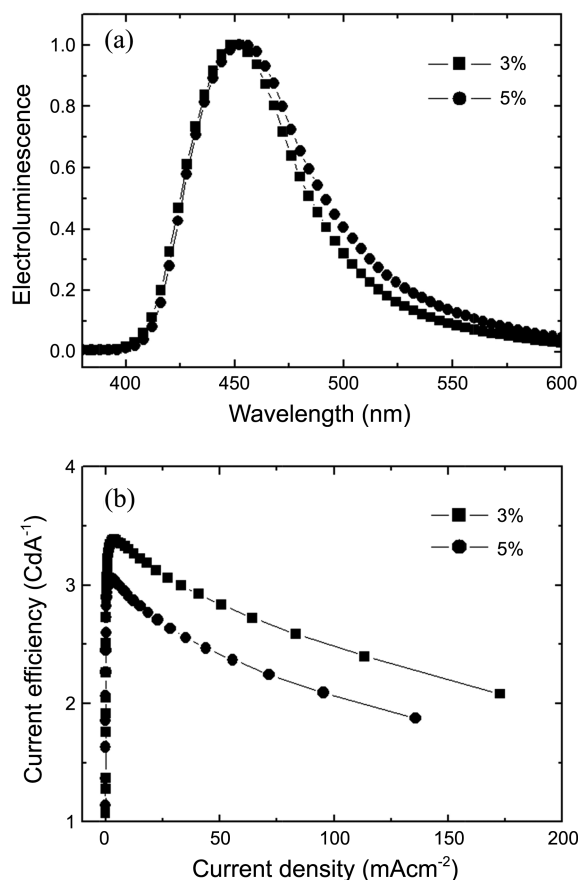
stable cation radical generation, and a half oxidation potential ($E_{1/2,ox}$) of 0.71 V. The highest occupied molecular orbital (HOMO) energy values of **2-TNPA** and NPD were calculated to be $E_{HOMO} = [(1.4 \pm 0.1) \times (0.43) (4.6 \pm 0.08)$ eV$] = 5.20$ eV and $E_{HOMO} = [(1.4 \pm 0.1) \times (0.28) (4.6 \pm 0.08)$ eV$] = 5.02$ eV, respectively.[12]

To investigate the multifunctional properties of **2-TNPA** as an organic semiconductor, we used the compound to fabricate four types of organic electronic devices: blue- and green-emitting OLEDs, OSC, and OTFT. In order to investigate the blue-emitting property of **2-TNPA**, we fabricated blue-fluorescent OLED devices with a configuration of ITO/CuPc (10 nm)/NPD (60 nm)/emitting layer (50 nm)/Alq$_3$ (20 nm)/LiF (1 nm)/Al (100 nm). Emitting layers were prepared by coevaporating ADN as a fluorescent host with x wt % **2-TNPA** as a fluorescent dopant. Figure 4(a) shows the electroluminescence (EL) spectra at different doping ratios of **2-TNPA**. The EL spectra of both 3% and 5% **2-TNPA** doping devices show the blue emission centered at 456 nm, and Commission Internationale de L'Eclairage (CIE) coordinates of (0.16, 0.14) (Figure S1). These results indicate that hole-electron recombination takes place at the **2-TNPA** layer. The FWHMs of the EL spectra at both 3% and 5% **2-TNPA** doping levels are 57 nm and 64 nm, respectively.

Figure 2. UV and PL spectra of **2-TNPA** (0.02 mM) in CH$_2$Cl$_2$.
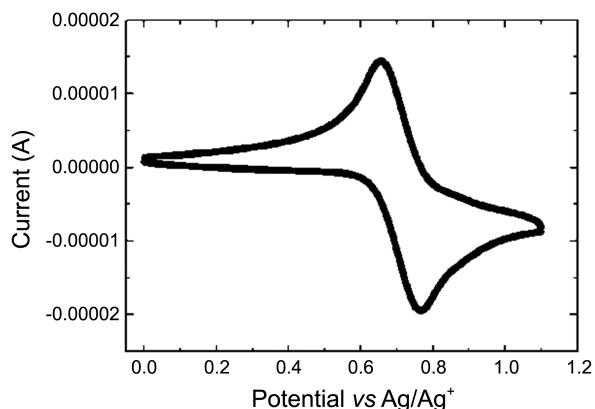
Figure 3. Cyclic voltammogram of 1.00 mM **2-TNPA** in CH$_2$Cl$_2$.

Table 1. Blue-emitting OLEDs device data

	η_p (lmW^{-1})^a	η_c (cdA^{-1})^b	η_{ext} (%)^c	EL (λ_{nm})^d	CIE
3%	1.21	3.42	3.01	456	(0.16, 0.14)
5%	1.16	3.06	2.92	456	(0.16, 0.14)

Device structure: ITO/CuPc (10 nm)/NPD (60 nm)/EML (50 nm)/Alq$_3$ (20 nm)/LiF (1 nm)/Al (100 nm). ^{a}Power efficiency. ^{b}Current efficiency. ^{c}External quantum efficiency. ^{d}Maximum EL emission.

Table 2. Green-emitting OLEDs device data

	η_p (lmW^{-1})^c	η_c (cdA^{-1})^d	η_{ext} (%)^e	EL (λ_{nm})^f	CIE
NPD^a	1.52	3.03	1.18	528	(0.34, 0.53)
2-TNPA^b	1.72	3.63	1.42	528	(0.34, 0.53)

^{a}ITO/NPD (70 nm)/Alq$_3$ (60 nm)/LiF (1 nm)/Al (100 nm). ^{b}ITO/**2-TNPA** (70 nm)/Alq$_3$ (60 nm)/LiF (1 nm)/Al (100 nm). ^{c}Power efficiency. ^{d}Current efficiency. ^{e}External quantum efficiency. ^{f}Maximum EL emission.

Since the FWHMs of PL and EL spectra are similar, we attribute the blue EL to the intrinsic emission of **2-TNPA**, with no emission interference from Alq$_3$. Because the EL spectra of **2-TNPA** devices with different doping ratios show similar patterns, it is suggested that the EL spectra should be attributed to an emission from an excited state of **2-TNPA** in the emitting layer.

Figure 4(b) shows the plots of current density (mAcm^{-2}) *vs.* current efficiency (cdA^{-1}) characteristics of the devices. The optimized 3% **2-TNPA**-doped device shows a maximum current efficiency of 3.0 cdA^{-1} and an external quantum efficiency of 3.0%. We attributed the improved current efficiency and external quantum efficiency to the greater charge balance and better exciton confinement within the emission layer. A comparison of the EL devices using **2-TNPA** as a
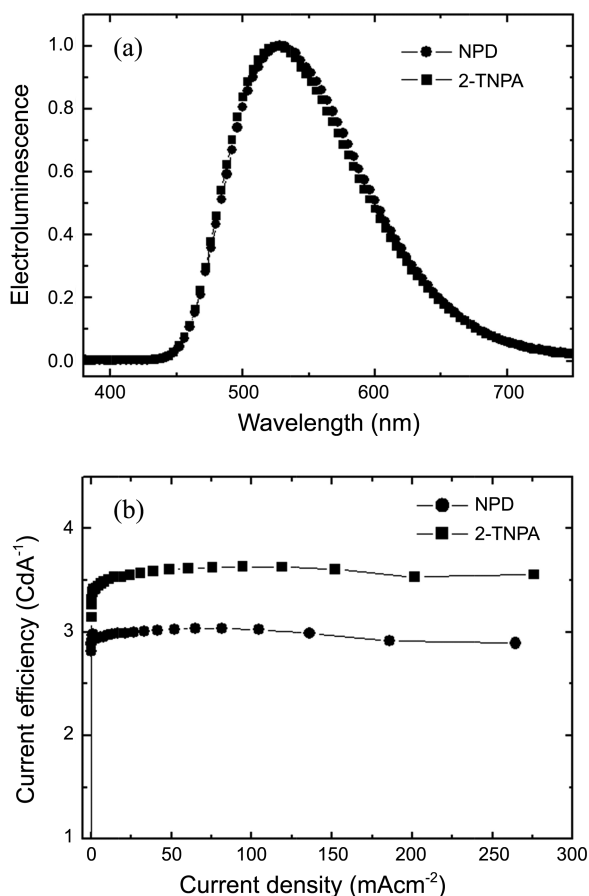

Figure 5. Green emitting OLED devices with a configuration of ITO/NPD or **2-TNPA** (70 nm)/Alq$_3$ (60 nm)/LiF (1 nm)/Al (100 nm). (a) EL spectra. (b) Current density (mAcm^{-2}) *vs.* current efficiency (cdA^{-1}) characteristics.

fluorescent dopant and the known blue- fluorescent dopant materials reveals that the current efficiency of 3.0 cdA^{-1} and the external quantum efficiency of 3.0% are generally good,[11] which indicates that **2-TNPA** can be used as an efficient blue-emitting material. In the 5% **2-TNPA** doping device, the current efficiency and external quantum efficiency are slightly decreased from 3.1 cdA^{-1} to 2.9 cdA^{-1} and from 3.1% to 2.9%, respectively. The slightly reduced current efficiency and external quantum efficiency can be attributed to a less balanced hole-and-electron recombination at the emitting layer caused by the aggregation of **2-TNPA** dopant molecules. The entire EL device data are summarized in Table 1 and Figure S2.

In order to compare the hole-transporting properties of **2-TNPA** and NPD, we fabricated two types of green- fluorescent OLEDs with the configuration of ITO/**2-TNPA** or NPD (70 nm)/Alq$_3$ (60 nm)/LiF (1 nm)/Al (100 nm). Figures 5(a) and S3 show the EL spectra and CIE coordinates of the NPD- and **2-TNPA**-based OLED devices. The EL spectra of both the **2-TNPA**- and NPD-based devices showed identical green emission centered at 528 nm, and almost equal CIE coordinates, which together suggest that the EL spectra and CIE coordinates should be attributed to an emission from an excited state of Alq$_3$ in the emitting layer. Figure 5(b) shows that the maximum current efficiency of the **2-TNPA**-based device is 3.6 cdA^{-1}, which is 20% higher than that of the NPD-based standard device (3.0 cdA^{-1}). Figure S4(d) shows that the external quantum efficiency of the **2-TNPA**-based device is 1.42%, which is 20% higher than that of the NPD-based standard device (1.18%). Enhancement of both current efficiency and external quantum efficiency as a result of using **2-TNPA** as the hole-transporting material can be attributed to better balanced charge recombination at the emitting layer. The HOMO (5.20 eV) energy level of **2-TNPA** is lower than that of NPD (5.02 eV), which results in a higher hole-blocking barrier that consequently retards hole transport in the **2-TNPA**-based device. Therefore, **2-TNPA** is a better hole-transporting material in green-emitting OLEDs than NPD.

In order to investigate the photovoltaic effect of **2-TNPA**, we fabricated OSCs with a configuration of ITO/ PEDOT: PSS (30 nm)/**2-TNPA** (x nm)/C$_{60}$ (40 nm)/BCP (5 nm)/Al (100 nm). Figure 6 shows the current–voltage (I–V) characteristics of **2-TNPA**- and C$_{60}$-based heterojunction solar cells under AM 1.5 simulated solar illumination. All the devices show photovoltaic behavior. The 10-nm thick **2-TNPA**-based device shows a short circuit current (I_{sc}) of 1.20 mAcm^{-2}, an open-circuit voltage (V_{oc}) of 0.46 V, and a
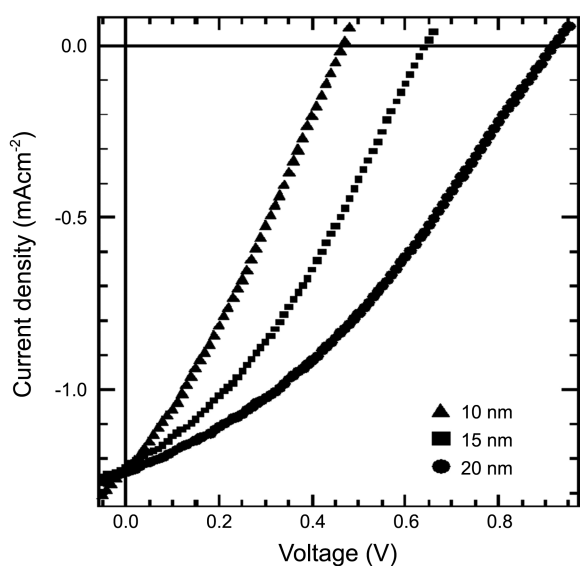
Figure 6. Current density–voltage characteristics of ITO/PEDOT (30 nm)/**2-TNPA** (*x* nm)/C_{60} (40 nm)/BCP (5 nm)/Al (100 nm) devices under simulated AM 1.5 irradiation at 100 mWcm^{-2}.

Table 3. OSC data

2-TNPA	V_{oc} (V)^a	I_{sc} (mAcm^{-2})^b	FF (%)^c	PCE (%)^d
10 nm	0.46	1.20	0.29	0.16
15 nm	0.64	1.30	0.33	0.28
20 nm	0.91	1.24	0.34	0.39

Device structure: ITO/PEDOT (30 nm)/**2-TNPA** (*x* nm)/C_{60} (40 nm)/Al (100 nm). ^{a}Open circuit voltage. ^{b}Short circuit current. ^{c}Fill factor. ^{d}Power conversion efficiency.

fill factor (FF) of 0.29. The low power-conversion efficiency (PCE) of 0.16% calculated from these data was attributed to the thin **2-TNPA** film, which reduced the absorption of the sunlight. The 15-nm thick **2-TNPA**-based device shows an I_{sc} of 1.30 mAcm^{-2}, a V_{oc} of 0.64 V, and an FF of 0.33. From these data, the power-conversion efficiency was calculated as 0.28%. The device with a 20-nm **2-TNPA** active layer shows an I_{sc} of 1.24 mAcm^{-2}, a V_{oc} of 0.91 V, and an FF of 0.34. From these data, the power-conversion efficiency was obtained as 0.39%. As a result, the change in the thickness of the **2-TNPA** film increased the power conversion efficiency from 0.16% to 0.39%. The OSC data of **2-TNPA**-based devices are summarized in Table 3.

In order to investigate the μ of **2-TNPA**, we fabricated an OTFT device using **2-TNPA** as an active material with a top-contact geometry. Figure 7 shows the output and transfer characteristics of top-contact OTFTs involving the use of **2-TNPA** deposited on SiO_2 and OTS/SiO_2 at a substrate temperature (T_{sub}) of 75 °C. From the electrical transfer characteristics, we obtained device parameters such as μ, the on/off current ratio (I_{on}/I_{off}), and V_{th}. All the devices show field effect transistor behavior. The **2-TNPA**-based OTFT device showed μ of 9.5×10^{-6} cm^{2}V^{-1}s^{-1}, a V_{th} of 19.6 V, and an I_{on}/I_{off} of 6.1×10^3 at 75 °C with bare SiO_2. The poor field-effect mobilities of the **2-TNPA**-based OTFT device
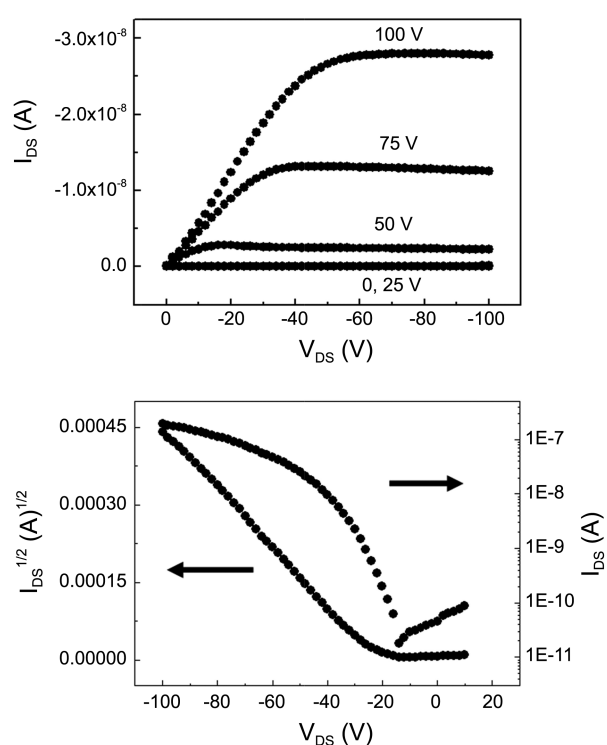

Figure 7. The output and transfer characteristics of the OTFTs involving the use of **2-TNPA** deposited at 75 °C OTS treated SiO_2.

Table 4. Data on OTFTs

2-TNPA	T_{sub} (°C)	μ (cm^{2}V^{-1}s^{-1})^a	V_{th} (V)^b	I_{on}/I_{off}^{c}
Bare SiO_2	RT	1.5×10^{-5}	-12.1	6.9×10^3
Bare SiO_2	75	9.5×10^{-6}	-19.6	6.1×10^3
OTS/SiO_2	RT	1.2×10^{-4}	-27.8	8.4×10^3
OTS/SiO_2	75	3.2×10^{-4}	-23.2	1.1×10^4

^{a}Field-effect mobility. ^{b}Threshold voltage. ^{c}On/off ratio.

can be attributed to the fact that it is difficult to maintain **2-TNPA** perpendicular to the substrate because of the three-dimensional star-shaped molecular structure of a triphenylamine unit and the poor crystalline morphology. Their morphological characteristics were investigated by X-ray diffraction (XRD). The thin-film XRD patterns of **2-TNPA** indicated no crystalline structure and a layer-by-layer molecular packing mode in **2-TNPA** on the substrate (Figure S5). On the other hand, with a more hydrophobic OTS-treated SiO_2 at 75 °C, the **2-TNPA**-based OTFT device showed an increased μ of 3.2×10^{-4} cm^{2}V^{-1}s^{-1}, a V_{th} of 23.2 V, and an I_{on}/I_{off} of 1.1×10^4. A μ of 3.2×10^{-4} cm^{2}V^{-1}s^{-1} in **2-TNPA**-based OTFT is slightly better than those in other three-dimensional star-shaped arylamine-based OTFTs.[6b] The OTFT data of the **2-TNPA**-based OTFT devices under various conditions are summarized in Table 4.

Conclusion

We have developed a new multifunctional material (**2-TNPA**) that can be used as a blue-emitting and hole-

transporting material in OLEDs, as well as a donor material in OSCs and an active material in OTFTs. The OLED device doped with 3% **2-TNPA** shows a maximum current efficiency of 3.0 cdA^{-1} and an external quantum efficiency of 3.0%. **2-TNPA** can be used as a more efficient hole-transporting material than NPD. Furthermore, **2-TNPA** shows a power-conversion efficiency of 0.39% in OSC and μ of 3.2 × 10^{-4} cm^{2}V^{-1}s^{-1} in OTFTs.

References

1. (a) Tang, C. W. *App. Phys. Lett.* **1986**, *48*, 183. (b) Tang, C. W.; Van Slyke, S. A. *App. Phys. Lett.* **1987**, *51*, 913. (c) Tsumura, A.; Koezuka, H.; Ando, T. *App. Phys. Lett.* **1986**, *49*, 1210.

2. (a) Anthony, J. E. *Chem. Rev.* **2006**, *106*, 5028. (b) Shirota, Y. *J. Mater. Chem.* **2005**, *15*, 75. (c) Shirota, Y. *J. Mater. Chem.* **2000**, *10*, 1. (d) Roncali, J. *Acc. Chem. Res.* **2009**, *42*, 1719.

3. (a) Lloyd, M. T.; Mayer, A. C.; Subramanian, S.; Mourey, D. A.; Herman, D. J.; Bapat, A. V.; Anthony, J. E.; Malliaras, G. G. *J. Am. Chem. Soc.* **2007**, *129*, 9144. (b) Roquet, S.; Cravino, A.; Leriche, P.; Alévêque, O.; Frère, P.; Roncali, J. *J. Am. Chem. Soc.* **2006**, *128*, 3459. (c) Kageyama, H.; Ohishi, H.; Tanaka, M.; Ohmori, Y.; Shirota, Y. *Adv. Funct. Mater.* **2009**, *19*, 3948. (d) Kwon, J.; Lee, W.; Kim, J.-y.; Noh, S.; Lee, C.; Hong, J.-I. *New J. Chem.* **2010**, *34*, 744. (e) Kwon, J.; Hong, J.-P.; Noh, S.; Kim, T.-M.; Kim, J.-J.; Lee, C.; Lee, S.; Hong, J.-I. *New J. Chem.* **2012**, *36*, 1813.

4. (a) Kim, Y.-H.; Jeong, H.-C.; Kim, S.-H.; Yang, K.; Kwon, S.-K. *Adv. Funct. Mater.* **2005**, *15*, 1799. (b) Chien, C.-H.; Chen, C.-K.; Hsu, F.-M.; Shu, C.-F.; Chou, P.-T.; Lai, C.-H. *Adv. Funct. Mater.* **2009**, *19*, 560.

5. (a) Tong, Q.-X.; Lai, S.-L.; Chan, M.-Y.; Lai, K.-H.; Tang, J.-X.; Kwong, H.-L.; Lee, C.-S.; Lee, S.-T. *Chem. Mater.* **2007**, *19*, 5851. (b) Li, J.; Liu, D.; Li, Y.; Lee, C.-S.; Kwong, H.-L.; Lee, S. *Chem. Mater.* **2005**, *17*, 1208. (c) Jiang, Z.; Liu, Z.; Yang, C.; Zhong, C.; Qin, J.; Yu, G.; Liu, Y. *Adv. Funct. Mater.* **2009**, *19*, 3987. (d) Moorthy, J. N.; Venkatakrishnan, P.; Huang, D.-F.; Chow, T. J. *Chem. Commun.* **2008**, 2146.

6. (a) Okamoto, H.; Kawasaki, N.; Kaji, Y.; Kubozono, Y.; Fujiwara, A.; Yamaji, M. *J. Am. Chem. Soc.* **2008**, *130*, 10470. (b) Sonntag, M.; Kreger, K.; Hanft, D.; Strohriegl, P.; Setayesh, S.; Leeuw, D. d. *Chem. Mater.* **2005**, *17*, 3031.

7. (a) Berggren, M.; Nilsson, D.; Robinson, N. D. *Nat. Mater.* **2007**, *6*, 3. (b) Kwon, J.; Hong, J.-P.; Lee, W.; Noh, S.; Lee, C.; Lee, S.; Hong, J.-I. *Org. Electron.* **2010**, *11*, 1103.

8. (a) Pandey, A. K.; Nunzi, J.-M. *Adv. Mater.* **2007**, *19*, 3613. (b) Lu, J.; Xia, P. F.; Lo, P. K.; Tao, Y.; Wong, M. S. *Chem. Mater.* **2006**, *18*, 6194.

9. (a) Cravino, A.; Roquet, S.; Alévêque, O.; Leriche, P.; Frère, P.; Roncali, J. *Chem. Mater.* **2006**, *18*, 2584. (b) Wang, F.; Luo, J.; Yang, K.; Chen, J.; Huang, F.; Cao, Y. *Macromolecules* **2005**, *38*, 2253.

10. (a) Kwon, J.; Kim, M. K.; Hong, J.-P.; Lee, W.; Noh, S.; Lee, C.; Lee, S.; Hong, J.-I. *Org. Electron.* **2010**, *11*, 1288. (b) Kim, M. K.; Kwon, J.; Hong, J.-P.; Lee, S.; Hong, J.-I. *Bull. Korean Chem. Soc.* **2011**, *32*. 2899.

11. Moorthy, J. N.; Venkatakrishnan, P.; Natarajan, P.; Huang, D.-F. Chow, T. J. *J. Am. Chem. Soc.* **2008**, *130*, 17320.

12. D'Andrade, B. W.; Datta, S.; Forrest, S. R.; Djurovich, P.; Polikaropov, E.; Thompson, M. E. *Org. Electron.* **2005**, *6*, 11.